Available online at www.sciencedirect.com
ScienceDirect
Journal of Solid State Chemistry 180 (2007) 702–712
JOURNAL OF SOLID STATE CHEMISTRY
www.elsevier.com/locate/jssc

Quantum chemical and spectroscopic analysis of calcium hydroxyapatite and related materials

V.D. Khavryuchenko[a], O.V. Khavryuchenko[b], V.V. Lisnyak[b,*]

[a]*Institute for Sorption and Problem of Endoecology, National Academy of Sciences of Ukraine, 13 General Naumov Str., 03164 Kyiv, Ukraine*
[b]*Kyiv National Taras Shevchenko University, 64 Volodymyrska Str., 01033 Kyiv, Ukraine*

Received 26 September 2006; received in revised form 23 November 2006; accepted 25 November 2006
Available online 5 December 2006

Abstract

Amorphous calcium hydroxyapatite was examined by vibrational spectroscopy (Raman and infra-red (IR)) and quantum chemical simulation techniques. The structures and vibrational (IR, Raman and inelastic neutron scattering) spectra of PO_4^{3-} ion, $Ca_3(PO_4)_2$, $[Ca_3(PO_4)_2]_3$, $Ca_5(PO_4)_3OH$, $CaHPO_4$, $[CaHPO_4]_2$, $Ca_3(PO_4)_2 \cdot H_2O$, $Ca_3(PO_4)_2 \cdot 2H_2O$ and $Ca_3(PO_4)_2 \cdot 3H_2O$ clusters were quantum chemically simulated at *ab initio* and semiempirical levels of approximation. A complete coordinate analysis of the vibrational spectra was performed. The comparison of the theoretically simulated spectra with the experimental ones allows to identify correctly the phase composition of the amorphous calcium hydroxyapatite and related materials. The shape of the bands in the IR spectra of the hydroxoapatite can be used in order to characterize the structural properties of the material, e.g., the PO_4^{3-} ion status, the degree of hydrolysis of the material and the presence of hydrolysis products.

Keywords: Cluster approximation; Calcium orthophosphate; Hydroxyapatite; Quantum chemical simulation; Ab initio; Normal coordinate analysis

1. Introduction

Calcium hydroxyapatite ($Ca_5(PO_4)_3OH$)-based composite materials (Ca–HAP) are widely used in biomedical engineering due to their compatibility with biological tissues and high cohesion and adhesion with metallic prosthesis [1–4]. The Ca–HAP properties are related to the chemical and structural peculiarities of the materials, e.g., the Ca/P ratio, porosity and crystallinity. The Ca–HAP materials can be manufactured by numerous technologies, in particular, by plasma spray deposition (PSD), producing a thin layer of nanoscale particles [5]. However, the Ca–HAP manufactured by the PSD possesses technological polymorphism [1] and commonly contains several minor semiamorphous heterogeneous phases, namely, CaO, $Ca(OH)_2$, $CaHPO_4$ and $Ca_3(PO_4)_2$, that affect the biological tissue properties [6].

The Ca–HAP materials processing requires a cheap and fast method to check the fitness of new technologies used. Infra-red (IR) spectroscopy meets the demands, being sensitive to the chemical and structural nature and mutual transformation of components in both the Ca–HAP materials as well as in the native bone tissue [1,2,7–11]. The phosphate components of the Ca–HAP materials can be identified and the content of the phosphate's hydrolysis products, effecting the acidity and mechanical properties of the tissues, can be characterized by IR spectroscopy, since the vibrations of Ca–O, orthophosphate and different hydroxyl groups are characteristic, sensitive to intra- and intermolecular interactions and the degree of crystallinity. The efficiency of spectroscopic testing rises substantially with the application of different vibrational techniques, including IR and Raman vibrational microspectroscopy and "chemical imaging". Additionally, an application of inelastic neutron scattering (INS) increases reliability of the spectra band assignment, especially for vibrations with a high level of hydrogen atom participation [12].

The spectroscopic characteristics of the technically optimal Ca–HAP samples already have been obtained [1].

*Corresponding author. Fax: +380 44 56 34274.
E-mail addresses: vkhavr@compchem.kiev.ua (V.D. Khavryuchenko), alexk@univ.kiev.ua (O.V. Khavryuchenko), lisnyak@chem.univ.kiev.ua (V.V. Lisnyak).

0022-4596/$ - see front matter © 2006 Elsevier Inc. All rights reserved.
doi:10.1016/j.jssc.2006.11.030

But the structure of the Ca–HAP materials is still questionable, and, therefore, the technological process cannot be theoretically optimized. The obstacle with converting the IR-spectroscopic data into structural information lies in the fact that the IR spectrum of the Ca–HAP cannot be presented as the superposition of the minor phases' IR spectra. This problem can be solved by applying quantum chemistry (QC) modelling, which allows the simulation of a space structure and the IR, Raman and INS spectra of the Ca–HAP materials. However, the literature data on QC calculations of the calcium-containing compounds are scant. A set of problems with assignment of the experimentally observed bands is also encountered. The vibrational spectra of the primary species of the Ca–HAP components should be theoretically assigned before analysis of the Ca–HAP material.

The simulation of the space structure and vibrational spectra of the primary species of the Ca–HAP, namely PO_4^{3-}, $Ca_3(PO_4)_2$, $CaHPO_4$, $Ca_5(PO_4)_3OH$ and hydrated $Ca_3(PO_4)_2$, can clarify the structure–property relations for the vibration spectra of the Ca–HAP materials. The comparison of the QC-derived and experimentally measured vibrational spectra allows to verify the theoretical computations and explain the experimental data. Vibrational spectroscopy was chosen as the method of experimental verification of QC-simulated data, since the direct methods of X-ray crystallography are not applicable in the case of amorphous nano-sized particles with a high level of interfacial interaction.

FTIR and Raman spectra of the hydroxyapatite ($Ca_5(PO_4)_3OH$) were recorded to verify the simulated vibrational spectra. Also, the data on the vibrational structure of the PO_4^{3-} ion taken from [13] and the INS spectrum of the hydroxoapatite ($Ca_5(PO_4)_3OH$) taken from [14] were used.

2. Materials

Commercial high purity hydroxyapatite ($Ca_5(PO_4)_3OH$) was purchased from Sigma-Aldrich (Catalog no. 289396) and was used without additional treatment.

3. Methods

3.1. Spectroscopic characterization

A Fourier transform Raman spectrometer Perkin-Elmer 1760 operating with ca. 50 mW Nd–YAG laser (Spectron, the wavelength of exciting beam is 1064 nm, the spectral resolution is 4 or 8 cm^{-1}) and an InGaAs detector was used for Raman spectra recording of the Sigma-Aldrich hydroxyapatite in the range of 3000–100 cm^{-1}. The samples were held in a brass sample holder in 180° backscattering geometry and nitrogen cooling was used.

The Fourier-transformed infra-red (FTIR) spectra of the Sigma-Aldrich hydroxyapatite were recorded on a Nicolette 320X FTIR spectrometer.

3.2. Computational methodology

3.2.1. Quantum chemical methodology

The QC study of the compound composing the Ca–HAP materials with the following formula, namely PO_4^{3-}, $Ca_3(PO_4)_2$, $[Ca_3(PO_4)_2]_3$, $Ca_5(PO_4)_3OH$, $CaHPO_4$, $[CaHPO_4]_2$, $Ca_3(PO_4)_2 \cdot H_2O$, $Ca_3(PO_4)_2 \cdot 2H_2O$ and $Ca_3(PO_4)_2 \cdot 3H_2O$, was performed using a semiempirical PM3 Hamiltonian [15] with the parameter set of [16] and *ab initio* methods [17,18]. The PM3 computations were performed in the framework of self-developed computation software for the cluster simulation "QuChem" [19]. MINI basis without polarization d-function, MINI-d1 basis with one polarization d-function and STO 6G-311 basis sets, introduced into PC-GAMESS software [17,18], were used for *ab initio* calculations.

The first step of QC examinations is local minimum optimization, since the potential function expansion and its approximation by the square-law function requires that the linear part of this expansion should be equal to zero. Therefore, the experimental structural data should be optimized before force-field evaluation. All QC calculations were performed up to complete structure optimization, Cartesian force-field evaluation, and dipole moment and polarisability derivatives calculation.

3.2.2. Vibrational spectra evaluation

COSPECO software [20] was used to simulate the vibrational spectra. The experimental spectra were used to solve the inverted vibration problem for the QC-simulated clusters. Three types of vibrational spectra were simulated, namely, IR, Raman and INS.

The theoretical vibrational spectra were obtained as sum of Gauss-like lines normalized to 100%. The pre-exponential coefficients of the Gauss-like lines were taken to be equal to computed intensities. The positions of the Gauss-like lines were stated to be equal to computed normal vibration frequencies and the line half-widths were defined by the type of the spectrum (IR, Raman or INS). After plotting of the theoretical spectra, the values of the half-widths were varied slightly to achieve a better agreement with the experimental ones. For the INS spectra, the half-widths were taken to be equal to known apparatus function [21]. The starting half-widths of the Gauss-like lines used for the IR and Raman spectra simulation were taken to be equal to 10 cm^{-1}. The inverted vibrational problems were solved in the internal dependent coordinate system for IR, Raman and INS spectra of all QC-simulated clusters.

The scaling factors for the studied clusters were derived by the fitting–scaling–fitting procedure, described in Section 3.2.

The comparison of the theoretically evaluated spectra with experimental ones was used to verify the validity of the simulated clusters, according to the "technology-following" methodology reported in [19,22]. Since the QC-simulated spectra of the phosphate clusters represent the vibrations of the simple molecular systems without the

effect of a solid-state surround, the inverted vibrational problem may be solved against the experimental spectra of both crystalline and amorphous samples. The crystalline hydroxyapatite was chosen as a reference, as its vibrational spectra are more resolved.

4. Results and discussion

4.1. Cluster description

The validity of the QC methods applied to the stated problem was tested. The Ca-containing clusters, simulated by the semiempirical PM3 method, were found to be unrealistic, forming artefacts of small calcium aggregates with Ca–Ca bonds and oxygen–oxygen peroxo-linkage between the orthophosphate groups. The calcium aggregates and the orthophosphate groups, simulated by PM3 method, are neutral, which contradict their chemical nature.

Therefore, only *ab initio* results are discussed further. The clusters PO_4^{3-}, $Ca_3(PO_4)_2$, $[Ca_3(PO_4)_2]_3$, $Ca_5(PO_4)_3OH$, $CaHPO_4$, $[CaHPO_4]_2$, $Ca_3(PO_4)_2 \cdot H_2O$, $Ca_3(PO_4)_2 \cdot 2H_2O$ and $Ca_3(PO_4)_2 \cdot 3H_2O$ were studied in order of increasing complexity of the units. The PO_4^{3-}, $Ca_3(PO_4)_2$ and $Ca_5(PO_4)_3OH$ clusters were considered in order to evaluate the scaling factors for the vibrational spectra of Ca–HAP. The $CaHPO_4$, $Ca_3(PO_4)_2 \cdot H_2O$, $Ca_3(PO_4)_2 \cdot 2H_2O$ and $Ca_3(PO_4)_2 \cdot 3H_2O$ clusters were simulated to study the impact of the acidic OH-groups on the vibrational spectra of the Ca–HAP. The $[Ca_3(PO_4)_2]_3$ and $[CaHPO_4]_2$ clusters were simulated in order to consider the effect of the cluster growth on the bond lengths and orders.

The orthophosphate anion PO_4^{3-} was simulated to test the fitting–scaling–fitting procedure and to obtain scaling factors for the orthophosphate anion in more complex clusters.

The geometry of the *ab initio*-simulated PO_4^{3-} ion is the ideal tetrahedron. The space and electronic structure data for orthophosphate anion are presented in Table 1. These results show that the P–O bond length values in the clusters, simulated in MINI and MINI-d1 bases, are considerably overstated and understated than the experimentally observed values equal to 1.510–1.550 Å [23], respectively. Yet, the STO 6G-311 basis gives the most correct result.

The $Ca_3(PO_4)_2$ cluster is a complex object possessing *ab initio*-proved 89 starting space structures corresponding to different topologies that combine three calcium cations and two orthophosphate anions [24]. The $Ca_3(PO_4)_2$ topologies were generated accounting for two basic principles: (1) four-fold O-coordinated P in PO_4-groups and (2) the electroneutrality principle. The topologies found differ by the ways in which the calcium and oxygen atoms are connected.

Table 1
Structural parameters of the PO_4^{3-} ion

Parameter	MINI basis set	MINI-d1 basis set	STO-6-311 basis set
d(P–O) (Å)	1.8095	1.5878	1.6409
P–O bond order	0.9450	1.5170	1.0910
q_P	0.5560	0.4510	1.8463
q_O	−0.8890	−0.8627	−1.2116

Two isomers of the $Ca_3(PO_4)_2$ with the highest and reduced symmetries, chosen for the examination, are presented in Fig. 1(a, b). Cluster 1 Fig. 1(a) $Ca_3(PO_4)_2$ of D_{3h} symmetry is the most stable isomer with three calcium atoms bridging two PO_4 groups. It was QC-simulated in both MINI and MINI-d1 *ab initio* bases sets. The $P–O^E$ (external) bond not coordinated to the Ca^{2+} ion, simulated in MINI-d1 basis, is considerably shorter than observed experimentally, due to the overestimation of the atomic *d*-orbitals' contribution into the binding molecular orbitals. The *ab initio*-computed structural and electronic data in cluster 1 are presented in Table 2. Cluster 2, Fig. 1(b) $Ca_3(PO_4)_2$ of C_{2v} symmetry was simulated in MINI basis set for comparison with Cluster 1. The Ca^{2+} ions occupy non-equivalent positions in this cluster: two Ca^{2+} ions have shorter contacts with the oxygens of orthophosphate groups. Due to the presence of four more covalent Ca–O bonds, cluster 2 is by 92.93 kcal/mol (basis set MINI) less energetically preferable than cluster 1.

The QC-simulated structure of the trimer of cluster 1 $[Ca_3(PO_4)_2]_3$ is shown in Fig. 1(c). The coordination number of the Ca^{2+} ion is 4–5, i.e. the Ca^{2+} ion is coordinationally unsaturated. The Ca^{2+} ion tends to increase its coordination number to the maximum of 12 by reacting with water and, hence, to the amorphization of the material.

Two molecules with different types of OH-groups were *ab initio*-simulated. The simplest Ca–HAP cluster with the formula $Ca_5(PO_4)_3(OH)$ contains hydroxyl groups bonded to the Ca^{2+} ion (Fig. 1(d)). The $CaHPO_4$ molecule (Fig. 1(e)) and its dimer $[CaHPO_4]_2$ (Fig. 1(f)) contain acidic OH-groups with the P–O bond order decreasing to the value of 0.698 and with the QC-calculated P–O distance equal to 1.756 Å. The O–H bond order in the $[CaHPO_4]_2$ dimer remains high, equal to 0.902, with the O–H distance of 0.988 Å.

Finally, the reactions of the $Ca_3(PO_4)_2$ cluster 1 with one, two and three molecules of water were QC-simulated in MINI basis, resulting in $Ca_3(PO_4)_2 \cdot H_2O$, $Ca_3(PO_4)_2 \cdot 2H_2O$ and $Ca_3(PO_4)_2 \cdot 3H_2O$ clusters (Figs. 1(g–i)). The reactions occur without an energetic barrier. Hydrolysis of the orthophosphate ions leads to the formation of acidic P–O–H and basic Ca–O–H groups. The proton of the acidic OH-group is situated in the two-well potential between oxygen atoms of the phosphate group and water, with the corresponding H–O distances 1.025–1.198 and 1.215–1.553 Å and bond orders 0.410 and 0.445, respectively. The impact of this phenomenon on the IR spectra is discussed below.

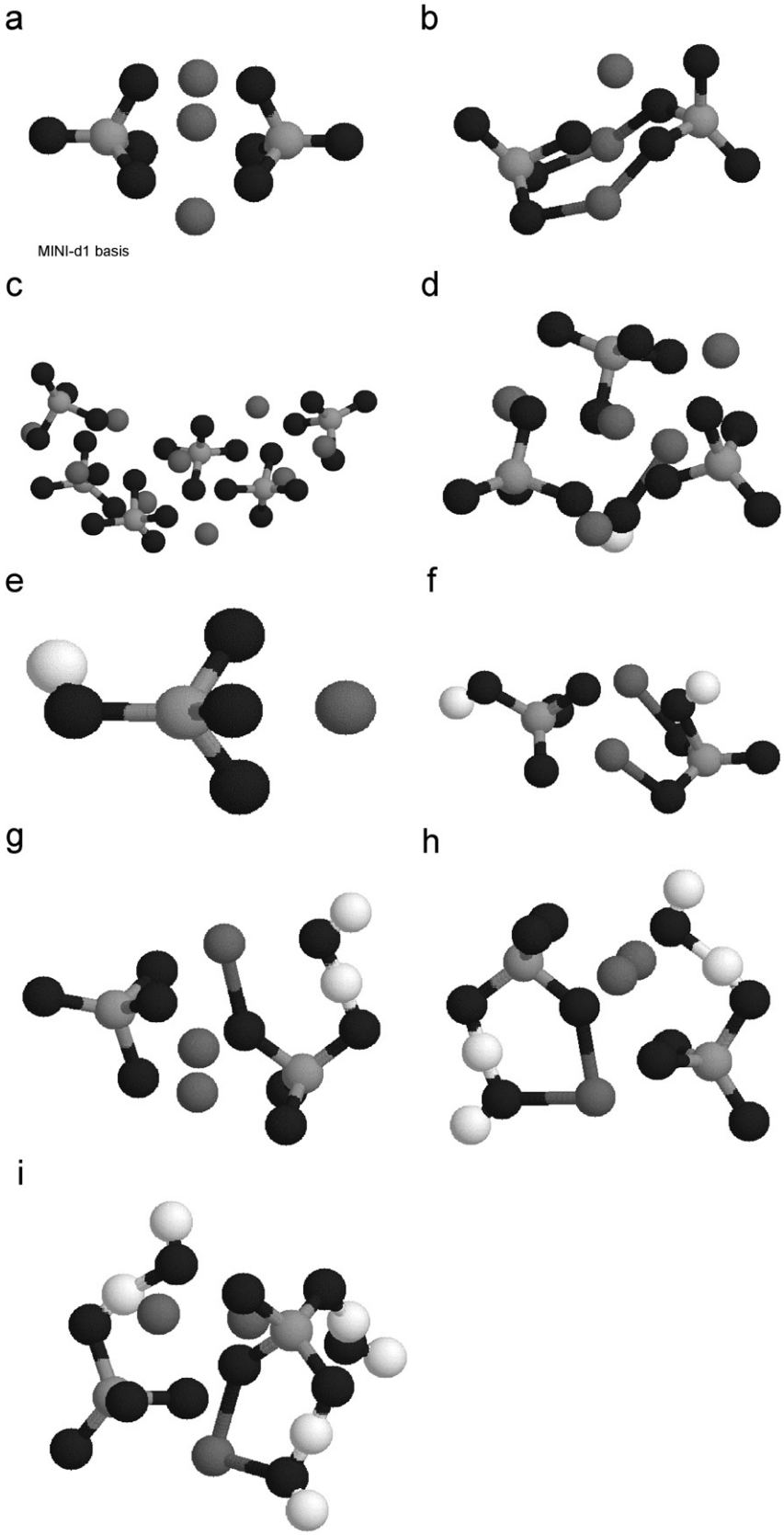

Fig. 1. The structures of calcium orthophosphates: $Ca_3(PO_4)_2$ cluster 1 (a) and cluster 2 (b), of $[Ca_3(PO_4)_2]_3$ (c), $Ca_5(PO_4)_3(OH)$ (d), $CaHPO_4$ (e), $[CaHPO_4]_2$ (f), $Ca_3(PO_4)_2 \cdot H_2O$ (g), $Ca_3(PO_4)_2 \cdot 2H_2O$ (h) and $Ca_3(PO_4)_2 \cdot 3H_2O$ (i) clusters, as quantum chemically optimized. Black is oxygen, white is hydrogen, light grey is phosphorus, dark grey is calcium.

4.2. Methodology of vibrational structure simulation

The results of *ab initio* simulations of the PO_4^{3-} ion, performed in the bases of MINI, MINI-d1 and STO 6G-311, were implemented in order to solve the inverted vibrational problem. The force field for the PO_4^{3-} ion was fitted to the experimental spectrum [13]. The calculated and experimental frequencies are congruent with high accuracy (deviation is less than $0.1\,cm^{-1}$). The calculated fitted force constants are listed in Table 3. Then, the scaling factors for the force constants of PO_4^{3-} ion vibration coordinates were derived by dividing the matrix elements of QC-calculated force constants by the matrix elements of fitted force constants.

The scaling factors of the PO_4^{3-} ion vibration coordinates were used to scale the QC-calculated spectra of the $Ca_3(PO_4)_2$ cluster. The spectra were fitted with respect to the experimental ones. The scaling factors of the vibrations involving the Ca^{2+} ion were modified. The new set of scaling factors was used to scale the QC-calculated spectra of the $Ca_5(PO_4)_3OH$ cluster. Then, the scaling factors for OH librations coordinate were modified.

The most important scaling factors are listed in Table 4.

The results of the study performed show that: (1) the scaling–fitting procedure is highly efficient for the Ca–HAP clusters and (2) the scaling factors of the vibrational spectra are invariant to the orthophosphate clusters. Since the vibration modes of the different groups of the HAP are slightly interdependent, the force constants of more complex systems need a slight fitting after application of the scaling factors, obtained for the simplified systems.

The force constants, simulated by *ab initio* methods in different basis sets, vary considerably. Therefore, the scaling factors are applicable within the same basis only.

4.3. Vibration spectra analysis

The simulated vibrational spectrum of the PO_4^{3-} anion was fitted to the experimental values $\nu_1 = 938\,cm^{-1}$ (A_1), $\nu_2 = 420\,cm^{-1}$ (E), $\nu_3 = 1017\,cm^{-1}$ (F_2), $\nu_4 = 567\,cm^{-1}$ (F_2), taken from [13]. The simulated and the fitted force constants are listed in Table 3. The values, obtained from the *ab initio* calculations in MINI, MINI-d1 and STO 6G-311 bases, are shown.

The simulated vibrational spectra of the $Ca_3(PO_4)_2$ clusters are shown in Fig. 2. The simulated vibrational

Table 2
Structural and electronic parameters of the $Ca_3(PO_4)_2$ cluster 1

Parameter	Basis set MINI	Basis set MINI-d1
d(P–O), (Å)/bond order	1.730/0.902	1.609/1.270
d(P = O), (Å)/bond order	1.696/1.103	1.472/1.925
d(Ca–O), (Å)/bond order	2.312/0.150	2.311/0.273
∠O = P–O (deg.)	120.80	116.90
∠O–P–O (deg.)	96.12	101.14
q_{Ca}	1.593	1.348
q_P	0.945	0.717
Q_{O-}	−0.901	−0.709
$Q_{O=}$	−0.631	−0.610

Table 4
Selected force constants of the cluster $Ca_5(PO_4)_3(OH)$ for the *ab initio* QC derived in MINI basis (QFF) and fitted force fields (FFF)

Force constant assignment	QFF constant ($10^6\,cm^{-2}$)	FFF constant ($10^6\,cm^{-2}$)	Scaling factor
K(P–O)	4.478857	8.851896	1.976374
K(P–O)Ca	2.797167	3.744483	1.338670
K(O–P–O)	0.611893	0.859452	1.404579
K(Ca–O)[a]	0.701218	0.803577	1.145973
K(Ca–O)[b]	1.099574	1.118851[c]	1.017532
K(O–H)	16.988580	13.037270	0.767414
K(Ca–O–H)	0.166450	0.289775	1.740915
K(P–O/P–O)[d]	−0.137331	−0.549269	3.999600

[a]4-fold coordinated Ca.
[b]3-fold coordinated Ca.
[c]average value.
[d]non-diagonal force constant.

Table 3
Force constants of the PO_4^{3-} ion

Force constant assignment	QFF constant in MINI basis ($10^6\,cm^{-2}$)	QFF constant in MINI-d1 basis ($10^6\,cm^{-2}$)	QFF constant in STO 6-311 basis ($10^6\,cm^{-2}$)	Fitted MINI	Fitted MINI-d1	Fitted 6-311
K(P–O)	3.3965	11.0926	8.1674	9.6522	9.7085	9.6877
K(P–O/P–O)[a]	–0.2680	0.6651	0.2806	1.0954	1.0766	1.0835
K(O–P–O)	1.4063	2.4303	2.1032	2.9504	1.9326	2.2458
K(P–O/O–P–O)[a]	0.0576	0.2957	0.2110	0.2402	0.2211	0.2267
K(P–O′/O–P–O)[a,b]	–0.0547	–0.2957	–0.2110	–0.2373	–0.2211	–0.2267
K(O–P–O/O–P–O)[a]	–0.2008	–0.3194	–0.2729	–0.1562	–0.3651	–0.3021
K(O′–P–O′/O–P–O)[a,b]	–0.5979	–1.1528	–1.0117	–0.8796	–0.8930	–0.8904

The force constants are given in the units $10^6\,cm^{-2}$. To convert the bond–bond force, the bond-angle force and the angle-angle force constants to mdin/Å, mdin and mdin · Å their values should be multiplied by factors 0.6409891, 0.6986781 and 0.7615592, respectively.
[a]non-diagonal force constant.
[b]P–O′ denotes coordinated to Ca^{2+}.

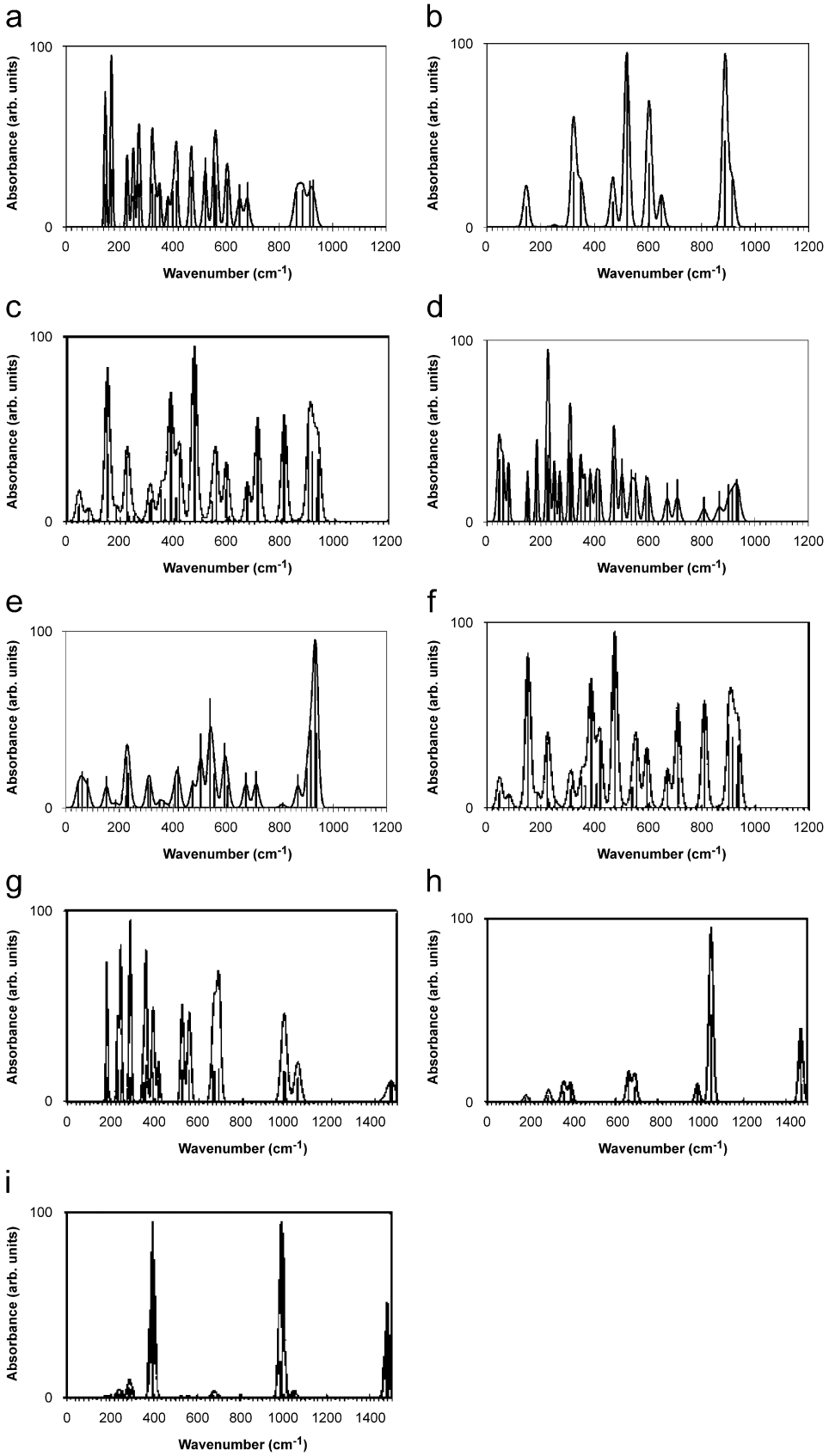

Fig. 2. The vibrational spectra of the $Ca_3(PO_4)_2$ clusters, simulated in MINI *ab initio* basis set: cluster 1 INS (a), IR (b) and Raman (c) spectra; cluster 2 INS (d), IR (e) and Raman (f) spectra. The vibrational spectra of the $Ca_3(PO_4)_2$ cluster 1, simulated in MINI-d1 *ab initio* basis set: INS (g), IR (h) and Raman (i) spectra.

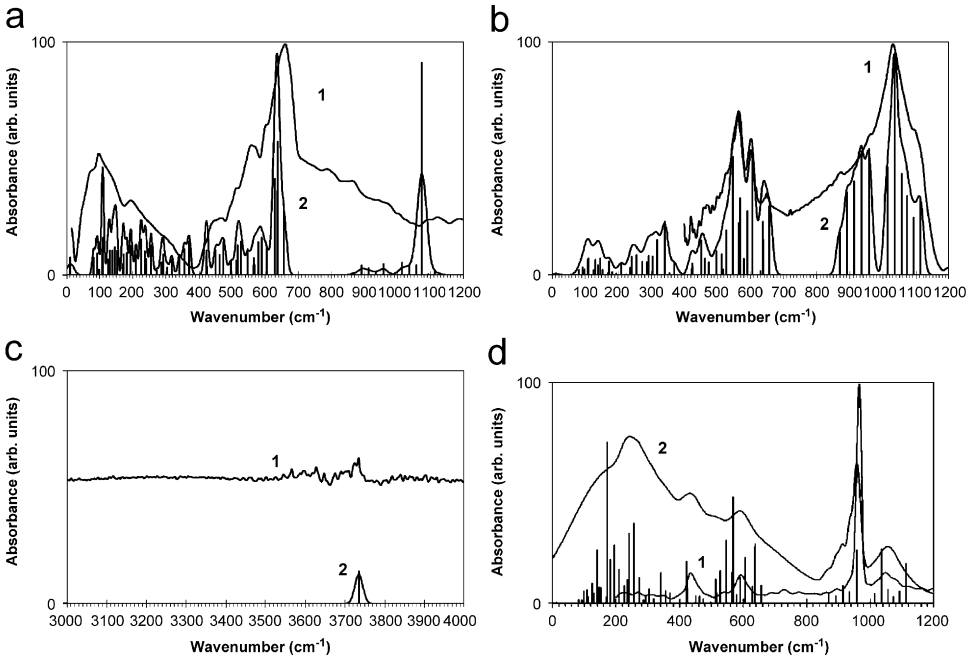

Fig. 3. The experimental (lines 1) and simulated (lines 2 and sticks) vibrational INS [25] (a), IR in mid-low frequency region (b), IR in high-frequency region (c) and Raman (d) spectra of the $Ca_5(PO_4)_3(OH)$ cluster.

structure of cluster 1 of the D_{3h} symmetry is strictly resolved. The bands, simulated from the model calculated in MINI basis, in regions 950–850 cm^{-1}, 650–600 cm^{-1}, 500–450 cm^{-1}, 400–350 cm^{-1} and 150 cm^{-1}, correspond to the v^{as}(P–O) originating from the F_2 vibration of the PO_4^{3-} anion, v^s(P–O) originating from the A_1 vibration of the PO_4^{3-} anion, δ(O–P–O) originating from the F_2 vibration of the PO_4^{3-} anion, δ(O–P–O) originating from the E vibration of the PO_4^{3-} anion, and (χ(Ca–O) + χ(P–O)) modes, respectively. The presence of the Ca^{2+} ions slightly disturbs the vibrational structure, splitting the bands and making the v^s(P–O) mode IR-active. The contribution of Ca–O vibration modes into orthophosphate group vibrations is negligible.

$Ca_3(PO_4)_2$ Cluster 2 with the C_{2v} symmetry has a more complicated vibrational structure due to the dissymmetry of the P–O bonds in different PO_4^{3-}groups. More modes are IR-active. The v^{as}(P–O) and δ(O–P–O) modes are additionally split. Still, the assignment of the bands is the same as for cluster 1.

As one can see, the calculated frequencies, referring to the model simulated in MINI basis, are significantly understated. On the contrary, the frequencies of the bands, simulated in MINI-d1 basis, are overstated. The application of the scaling factors, obtained from the fitting of the PO_4^{3-} anion in the corresponding basis, allows to shift the orthophosphate bands to the experimentally determined positions.

The simulated vibrational spectra of $Ca_5(PO_4)_3(OH)$ cluster are shown in Fig. 3. The scaling factors, evaluated from the $Ca_3(PO_4)_2$ vibrational spectra simulation, were applied to the calculated force constants of the

Table 5
QC calculated vibration spectra of the cluster $Ca_5(PO_4)_3OH$–hydroxoapatite: frequencies, relative intensities, potential energy distribution (PED) and bands assignment

No	Frequency (cm^{-1})	INS rel. int.	IR rel. int.	Raman rel. int.	PED (%)	Assignment
148	3735.00	100.00	14.45	78.07	99.94	$\nu_{O–H}$
147	1112.66	2.24	34.34	4.92	77.67	$\nu_{P–O}$
					11.18	$\nu_{P–O}$
146	1092.71	0.50	25.84	1.48	9.17	$\nu_{P–O}$
145	1073.64	96.00	35.77	0.79	51.34	$\delta_{Ca–O–H}$
144	1056.95	4.53	45.68	1.64	45.15	$\nu_{P–O}$
143	1035.60	4.63	100.00	6.70	56.84	$\nu_{P–O}$
142	1014.36	5.53	48.66	1.16	67.32	$\nu_{P–O}$
					5.97	$\delta_{O–P–O}$
					8.42	$\delta_{Ca–O–P}$
141	957.74	5.04	56.75	6.57	58.59	$\nu_{P–O}$
140	934.53	1.34	55.70	1.41	49.97	$\nu_{P–O}$
139	913.40	2.99	42.16	2.16	67.68	$\nu_{P–O}$
					7.11	$\delta_{O–P–O}$
138	892.09	4.35	37.32	0.85	16.24	$\nu_{P–O}$
					50.39	$\nu_{P–O}$
137	869.26	1.03	19.21	1.15	54.66	$\nu_{P–O}$
					6.68	$\delta_{Ca–O–P}$
136	656.59	32.15	30.92	2.24	15.00	$\nu_{P–O}$
135	637.96	60.29	15.73	7.31	38.50	$\rho_{Ca–O–Ca}$
134	636.54	37.98	23.88	7.03	19.79	$\nu_{P–O}$
133	629.42	43.55	1.74	2.09	21.55	$\rho_{Ca–O–Ca}$
132	604.94	12.28	54.31	5.63	14.74	$\nu_{Ca–O}$
					5.65	$\nu_{Ca–O}$
					32.66	$\nu_{P–O}$
					13.63	$\nu_{P–O}$
131	590.28	16.85	28.73	3.22	12.46	$\nu_{Ca–O}$
					12.29	$\nu_{Ca–O}$
					5.28	$\nu_{Ca–O}$

Table 5 (*continued*)

No	Frequency (cm^{-1})	INS rel. int.	IR rel. int.	Raman rel. int.	PED (%)	Assignment
					19.11	ν_{P-O}
					6.55	δ_{O-P-O}
130	579.71	14.74	7.23	1.08	5.57	ν_{Ca-O}
					19.75	ν_{Ca-O}
					33.94	ν_{P-O}
129	568.31	4.62	34.69	13.16	7.26	ν_{Ca-O}
					7.42	ν_{P-O}
					14.87	ν_{P-O}
128	565.47	7.70	10.69	3.30	17.19	ν_{P-O}
					14.98	ν_{P-O}
					9.66	δ_{O-P-O}
127	564.58	4.50	23.39	3.77	6.41	ν_{Ca-O}
					9.79	ν_{Ca-O}
					5.77	ν_{Ca-O}
					14.16	ν_{P-O}
					6.24	ν_{P-O}
126	547.03	11.52	53.15	7.77	13.44	ν_{Ca-O}
					13.33	ν_{Ca-O}
					15.11	ν_{P-O}
					5.52	δ_{O-P-O}
					13.04	δ_{O-P-O}
					7.86	δ_{Ca-O-P}
125	526.66	15.02	20.24	3.99	20.41	ν_{Ca-O}
124	517.61	13.37	2.41	1.28	13.59	ν_{Ca-O}
123	513.70	6.55	9.35	2.99	5.08	ν_{Ca-O}
					22.28	ν_{Ca-O}
122	496.60	6.42	10.63	0.14	11.99	ν_{Ca-O}
					6.78	ν_{Ca-O}
121	474.24	14.84	5.75	0.51	10.20	ν_{Ca-O}
					5.53	ν_{P-O}
					23.40	δ_{O-P-O}
					5.86	δ_{Ca-O-P}
120	462.53	9.14	7.38	0.86	10.18	ν_{Ca-O}
					6.74	ν_{Ca-O}
					10.34	ν_{P-O}
					6.33	δ_{O-P-O}
119	450.38	11.29	15.47	0.85	14.52	ν_{Ca-O}
118	424.41	3.86	3.81	1.89	23.81	ν_{Ca-O}
					16.93	ν_{P-O}
					16.33	δ_{O-P-O}
					6.27	δ_{O-P-O}
117	423.17	11.09	5.12	3.32	5.65	ν_{Ca-O}
					5.12	ν_{Ca-O}
					11.51	ν_{P-O}
					6.40	δ_{O-P-O}
116	421.99	8.66	2.61	5.13	9.59	ν_{Ca-O}
					11.12	ν_{P-O}
					9.06	δ_{O-P-O}
115	369.66	15.06	5.53	1.25	11.15	ν_{Ca-O}
114	355.73	11.52	0.82	1.55	9.59	ν_{Ca-O}
					5.95	ν_{P-O}
					11.57	δ_{O-P-O}
113	340.98	7.19	23.89	3.81	6.66	ν_{Ca-O}
					8.06	ν_{Ca-O}
112	317.66	6.80	15.69	0.56	10.76	ν_{Ca-O}
111	304.05	3.52	8.33	1.75	5.03	ν_{Ca-O}
					11.97	ν_{Ca-O}
					7.77	ν_{Ca-O}
110	292.33	9.41	8.59	0.85	11.06	ν_{Ca-O}
					7.94	ν_{Ca-O}
109	286.40	5.74	5.70	0.40	6.80	ν_{Ca-O}
					14.72	ν_{Ca-O}

Table 5 (*continued*)

No	Frequency (cm^{-1})	INS rel. int.	IR rel. int.	Raman rel. int.	PED (%)	Assignment
					5.16	ν_{Ca-O}
					5.76	δ_{O-P-O}
108	272.61	2.05	5.95	3.11	7.47	ν_{Ca-O}
					7.25	ν_{Ca-O}
					15.90	ν_{P-O}
107	255.65	13.24	8.95	9.91	19.79	ν_{Ca-O}
					9.60	ν_{Ca-O}
					10.74	ν_{P-O}
					10.00	δ_{O-P-O}
					5.35	δ_{Ca-O-P}
106	241.07	7.20	8.21	8.60	14.14	ν_{Ca-O}
					12.51	ν_{Ca-O}
					6.30	δ_{O-P-O}
105	235.74	10.58	3.14	2.95	6.80	ν_{Ca-O}
					7.49	δ_{O-P-O}
104	225.17	16.02	0.14	2.19	13.08	ν_{Ca-O}
					9.48	ν_{Ca-O}
					22.76	δ_{O-P-O}
					6.19	δ_{O-P-O}
103	209.83	8.97	5.44	4.21	5.10	ν_{Ca-O}
					5.86	ν_{Ca-O}
					9.23	δ_{O-P-O}
					11.57	δ_{O-P-O}
102	194.48	13.04	0.62	7.22	12.52	ν_{Ca-O}
101	181.53	9.78	1.31	5.41	9.69	ν_{Ca-O}
100	171.95	9.28	6.12	19.93	16.25	ν_{Ca-O}
					5.14	ν_{P-O}
99	169.68	5.02	0.80	0.74	10.10	ν_{Ca-O}
					19.33	δ_{O-P-O}
					6.06	δ_{Ca-O-P}
98	151.80	10.92	2.32	1.92	8.94	ν_{Ca-O}
					7.00	ν_{Ca-O}
					8.09	δ_{O-P-O}
					7.01	δ_{O-P-O}
					9.02	δ_{Ca-O-P}
					5.84	δ_{Ca-O-P}
97	145.94	12.65	7.40	1.98	15.08	δ_{O-P-O}
96	139.23	11.06	4.32	6.62	7.07	ν_{Ca-O}
					5.93	ν_{Ca-O}
					9.22	δ_{O-P-O}
95	130.43	11.11	6.66	1.23	6.46	δ_{O-P-O}
					10.63	δ_{Ca-O-P}
					6.72	δ_{Ca-O-P}
94	124.67	7.17	2.19	2.46	7.79	ν_{Ca-O}
					13.80	ν_{Ca-O}
93	110.53	16.91	7.36	0.81	10.70	ν_{Ca-O}
92	107.36	11.57	6.86	1.66	20.61	ν_{Ca-O}
					5.03	δ_{O-P-O}
					10.72	δ_{Ca-O-P}
91	98.72	2.40	2.49	1.46	6.78	ν_{Ca-O}
					7.99	ν_{P-O}
					7.09	δ_{O-P-O}
					9.77	δ_{Ca-O-P}
90	92.58	9.77	3.39	0.41	18.34	ν_{Ca-O}
89	82.11	7.89	2.26	0.47	10.22	χ_{Ca-O}
88	11.92	8.00	0.57	0.10	24.46	χ_{P-O}

Normal vibration notation: ν, stretch vibration, δ, angle deformation, ρ, out–of–plane vibration, χ, torsion vibration.

orthophosphate groups and vibrations, involving Ca^{2+} ion. Then, the simulated IR and INS spectra were fitted to the experimental ones, recorded by authors and taken from [14], respectively. Despite the small size, after application of the scaling–fitting procedure, the $Ca_5(PO_4)_3(OH)$ cluster can reproduce the main features of the Ca–HAP

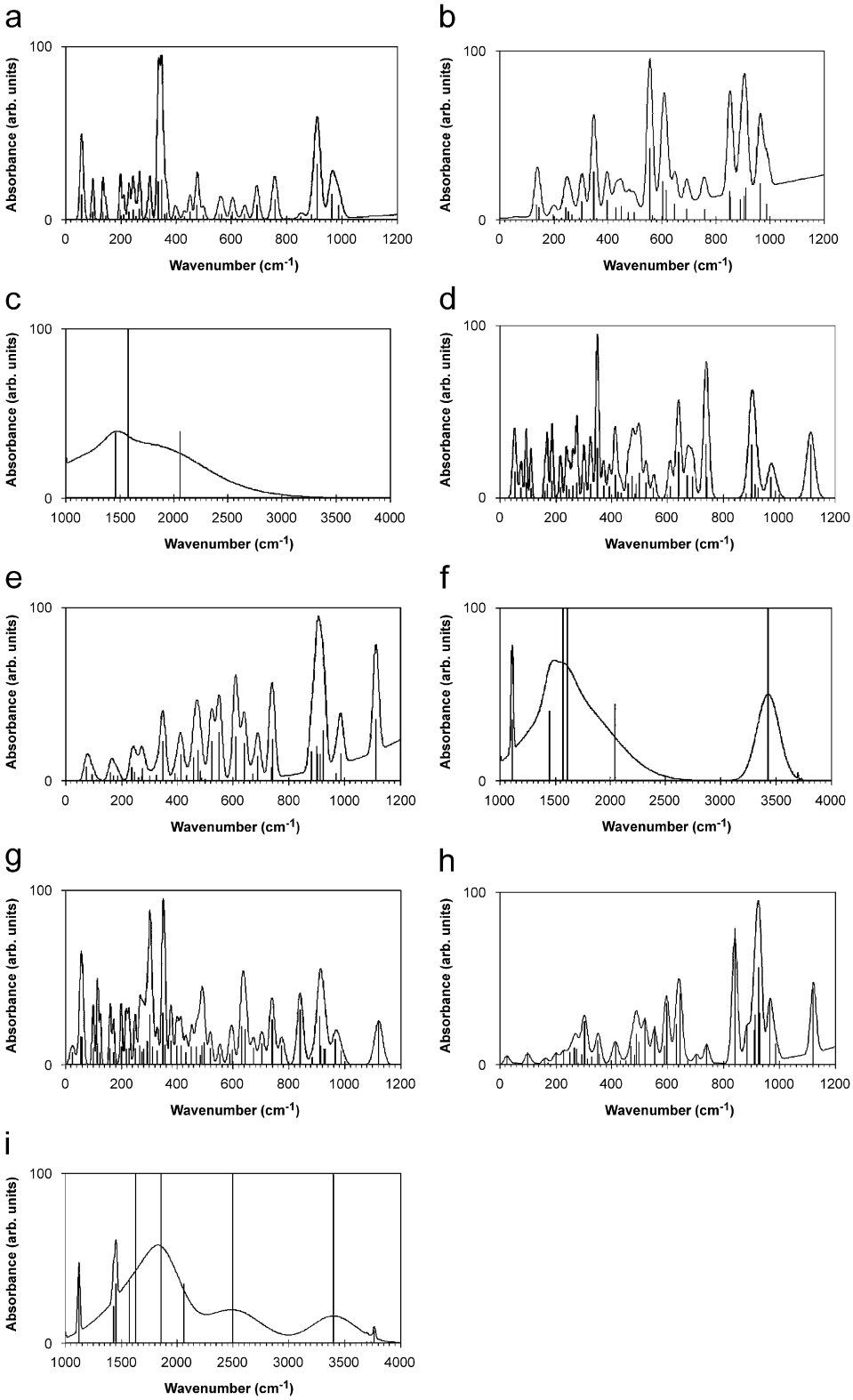

Fig. 4. The simulated vibrational spectra of the $Ca_3(PO_4)_2 \cdot xH_2O$ (where $x = 1$–3) clusters: INS (a), IR in mid-low-frequency region (b), IR in high-frequency region (c) of the $Ca_3(PO_4)_2 \cdot H_2O$ cluster; INS (d), IR in mid-low-frequency region (e), IR in high-frequeny region (f) of the $Ca_3(PO_4)_2 \cdot 2H_2O$ cluster; INS (g), IR in mid-low-frequency region (h), IR in high frequency region (i) of the $Ca_3(PO_4)_2 \cdot 3H_2O$ cluster.

experimental spectra, namely IR, Raman and INS, including the intensities of the vibrations. This has allowed the assigning of the OH group librations and to evaluate corresponding scaling factors (the most important scaling factors are shown in Table 4). The normal coordinate analysis of $Ca_5(PO_4)_3(OH)$ vibration frequencies is shown in Table 5.

As one can see, the ν(P–O) vibrations, observed in the region 1300–800 cm^{-1} are almost pure by form, without significant contribution of the vibrations involving Ca^{2+} ion. The influence of the Ca^{2+} ion consists in the splitting of the originally degenerated ν(P–O) vibrations. As a result, a smoothed halo is observed in this region of the INS spectra, and the wide band i.e. the envelope curve or sum of all normal vibration bands is observed in the IR spectrum instead of sharp peaks.

On the contrary, the δ(O–P–O) vibrations are influenced by the Ca^{2+} ion greatly. Almost all vibrations in the region below 600 cm^{-1} have the contribution of ν(Ca–O) or δ(Ca–O–P) modes.

The OH group riding on a Ca^{2+} ion has a few distinct sharp bands with the frequencies 3735 and 1073 cm^{-1}. The group of bands in the region 660–630 cm^{-1} have a great contribution of OH-group librations, which leads to the increase of the INS intensities.

The ν(H–O) band of the strongly hydrogen-bonded OH group of the $Ca_3(PO_4)_2 \cdot xH_2O$ (where $x = 1$–3) clusters (Fig. 4) is shifted to lower frequencies up to 1000 cm^{-1}, when comparing with $Ca_5(PO_4)_3(OH)$ due to a two-well potential character of the bridging hydrogen atom (see Section 3.1). Such a shift is accompanied by the growth of intensity and half-width of the band in the IR spectrum, which is in good agreement with the literature data of [25]. The increase of the half-width leads to the vanishing of the band due to the drift of the baseline.

Therefore, the shape of the bands in the IR spectra of the Ca–HAP can be used to characterize the structural properties of the material. The bands in the region 1300–800 cm^{-1} reflect the PO_4^{3-} ion status. The sharp splitted bands indicate the presence of the $Ca_3(PO_4)_2$ phase with a small content of the hydroxyl groups. The region 800–400 cm^{-1} is very sensitive to the status of the Ca^{2+} ions. The coordination type of the Ca^{2+} ion and the orthophosphate polyhedron transformations can be studied from the forms and intensities of the bands in this region. The spectral region below 400 cm^{-1} can be used to investigate cluster packing and bonding between the orthophosphate–calcium aggregates. Finally, the character of the ν(H–O) band can be used to check the degree of hydrolysis of the Ca–HAP material: the sharp band at 3600–3760 cm^{-1} in the IR spectra and intense band at 650 cm^{-1} of the INS spectra indicate the $Ca_5(PO_4)_3(OH)$, while a broad band below 3300 cm^{-1} is an evidence of the hydrolysis products' presence, namely $CaHPO_4$ with H-bonded OH groups.

Therefore, the QC simulation of the Ca–HAP vibrational spectra has allowed to assign the experimentally observed bands. The set of scaling factors for the corresponding force constants was evaluated. The scaling–fitting procedure has proved to be efficient. Since a sharp difference is observed between the Ca-coordinated and P–O^E (external) bonds, different scaling factors, should be applied to them. Thus, before applying the scaling factors, one needs to solve the inverted vibrational problem for the simplified model, mainly, in order to assign the fundamental vibrations. Using this procedure, it is possible to examine more complex Ca–HAP materials obtaining information about their structural properties.

5. Summary

The PO_4^{3-} ion, $Ca_3(PO_4)_2$, $[Ca_3(PO_4)_2]_3$, $Ca_5(PO_4)_3OH$, $CaHPO_4$, $[CaHPO_4]_2$, $Ca_3(PO_4)_2 \cdot H_2O$, $Ca_3(PO_4)_2 \cdot 2H_2O$ and $Ca_3(PO_4)_2 \cdot 3H_2O$ clusters were QC simulated. The *ab initio* calculations in the STO 6G-31111 basis have appeared to be the most relevant. The models, simulated in MINI and MINI-d1 bases, can also be used to study vibrational spectra of the Ca–HAP clusters. The semi-empirical PM3 method with the parameters of [16] is completely inefficient due to the incorrect Ca parameters.

The vibrational spectra, namely IR, Raman and INS, of the Ca–HAP clusters, were simulated, reproducing the experimental ones well. The complete vibration band analysis was performed. The vibrational bands were assigned. It was shown that the structural properties of the HAP phases can be evaluated from the features of the IR spectra. This could be used to control the manufacturing of the Ca–HAP materials and to manage their properties.

The scaling–fitting procedure, applied to the Ca–HAP systems, has proved to be highly efficient. The set of the scaling factors for the PO_4^{3-} ion, $Ca_3(PO_4)_2$ and $Ca_5(PO_4)_3(OH)$ clusters was evaluated. The scaling factors are invariant enough and can be easily transferred within the same basis set.

References

[1] M. Vallet-Regí, J.M. González-Calbet, Prog. Solid State Chem. 32 (2004) 1–31.
[2] G.N. Babini, A. Tampieri, Br. Ceram. Trans. 103 (2004) 101–109.
[3] M.P. Bolognesi, R. Pietrobon, P.E. Clifford, T.P. Vail, J. Bone Joint Surg. A 86 (2004) 2720–2725.
[4] J. Dumbleton, M.T. Manley, J. Bone Joint Surg. A 86 (2004) 2526–2540.
[5] R.X. Sun, Y.P. Lu, M.S. Li, Surf. Eng. 19 (2003) 392–394.
[6] V.N. Bagratashvili, E.N. Antonov, E.N. Sobol, V.K. Popov, S.M. Howdle, Appl. Phys. Lett. 66 (1995) 2451–2453.
[7] A. Bigi, E. Boanini, M. Gazzano, K. Rubini, P. Torricelli, Bio-Med. Mater. Eng. 14 (2004) 573–579.
[8] N. Ignjatovic, D. Uskokovic, Spectroscopy 18 (2004) 553–565.
[9] A. Slosarczyk, J. Piekarczyk, Ceram. Int. 25 (1999) 561–565.
[10] H. Zeng, W.R. Lancefield, Biomaterials 21 (2000) 21–30.
[11] M. Weinlaender, J. Beumer, E.B. Kenney, P.K. Moy, J. Mater. Sci.: Mater. Med. 3 (1992) 397–401.
[12] M.G. Taylor, K. Simkiss, S.F. Parker, P.C.H. Mitchell, Phys. Chem. Chem. Phys. 1 (1999) 3141–3144.

[13] K. Nakamoto, Infrared and Raman Spectra of Inorganic and Coordination Compounds (Infrared and Raman Spectra of Inorganic and Coordination Compounds, Theory and Applications in Inorganic Chemistry), fourth ed, Wiley Interscience, New York, 1997, p. 408.
[14] P.C.H. Mitchell, S.F. Parker, K. Simkiss, J. Simmons, M.G. Taylor, J. Inorg. Biochem. 62 (1996) 183–197.
[15] J.J.P. Stewart, J. Comput. Chem. 10 (1989) 221–264.
[16] www.hyper.com.
[17] M.W. Schmidt, K.K. Baldridge, J.A. Boatz, S.T. Elbert, M.S. Gordon, J.H. Jensen, S. Koseki, N. Matsunaga, K.A. Nguyen, S.J. Su, T.L. Windus, M. Dupuis, J.A. Montgomery Jr., J. Comput. Chem. 14 (1993) 1347–1363.
[18] www.msg.ameslab.gov/GAMESS/pcgamess.shtml.
[19] A.V. Khavryutchenko, V.D. Khavryutchenko, Z. Naturforsch. A 60 (2005) 41–47.
[20] V.D. Khavryutchenko, Eurasian ChemTech. J. 6 (2004) 157–170.
[21] I. Natkaniec, S.I. Bragin, J. Brankowski, J. Mayer, RAL Report No. 94–025, I, 1993, p. 89.
[22] O.V. Khavryuchenko, V.D. Khavryuchenko, J.O. Roszinski, A.I. Brusilovets, B. Friede, V.V. Lisnyak, Thin Solid Films 515 (2006) 1280–1285.
[23] D.E.C. Corbridge, Phosphorus, Elsevier, Amsterdam, 2000, p.1267.
[24] G. Treboux, N. Kanazaki, K. Onuma, A. Ito, J. Phys. Chem. A 103 (1999) 8118–8120.
[25] H. Ratajczak, W.J. Orville-Thomas, Molecular Interactions, Wiley, Chichester, NY, 1980.